Mortazavi Farzad (Orcid ID: 0000-0002-1911-5428)
Reidenberg Joy S. (Orcid ID: 0000-0002-4180-7156)
Hanke Frederike Diana (Orcid ID: 0000-0002-1737-3861)
Strobel Sarah McKay (Orcid ID: 0000-0002-5259-0589)

Specializations of somatosensory innervation in the skin of humpback whales (*Megaptera novaeangliae*)

Sherri A. Eldridge[1,2], Farzad Mortazavi[1], Frank L. Rice[3], Darlene R. Ketten[4], David N. Wiley[5], Ed Lyman[6], Joy S. Reidenberg[7], Frederike D. Hanke[8], Steffen DeVreese[9,10], Sarah McKay Strobel[11], Douglas L. Rosene[1]

[1] Department of Anatomy and Neurobiology, Boston University School of Medicine, Boston, MA 02118

[2] Biology Department, University of Massachusetts Dartmouth, Dartmouth, MA 02747

[3] Integrated Tissue Dynamics, Rensselaer, NY 12144

[4] Woods Hole Oceanographic Institution, Woods Hole, MA 02543

[5] National Oceanic and Atmospheric Administration/ National Ocean Service/Stellwagen Bank National Marine Sanctuary, Scituate, MA 02066.

[6] Hawaiian Islands Humpback Whale National Marine Sanctuary, Kihei, HI 96753

[7]Center for Anatomy and Functional Morphology, Icahn School of Medicine at Mount Sinai, New York, NY 10029-6574

[8] University of Rostock, Institute for Biosciences, Neuroethology, 18059 Rostock, Germany

[9] Department of Comparative Biomedicine and Food Science, University of Padova, Padova, Italy

[10] Laboratory of Applied Bioacoustics, Technical University of Catalonia, BarcelonaTech, Barcelona, Spain

[11] University of California Santa Cruz, Department of Ecology and Evolutionary Biology, Santa Cruz, CA 95060, USA

Corresponding Author: Farzad Mortazavi, PhD. 310-729-8830, farzad@bu.edu

Running Title: Innervation in the Skin of Humpback Whales

This is the author manuscript accepted for publication and has undergone full peer review but has not been through the copyediting, typesetting, pagination and proofreading process, which may lead to differences between this version and the Version of Record. Please cite this article as doi: 10.1002/ar.24856

Manuscript Correspondence:
Farzad Mortazavi
Department of Anatomy and Neurobiology
Boston University School of Medicine
700 Albany St., #W-701
Boston, MA 02118

Grants
Grant sponsor: National Ocean Service, Grant number: NA10SEC4810008 (to S.A.E); Grant sponsor: NIH, Grant numbers: R01-AG043640, R01-AG042512 (to D.L.R.), Grant sponsor: American Association of University Women, Grant: American Dissertation Fellowship (to S.A.E).

Abstract

Cetacean behavior and life history imply a role for somatosensory detection of critical signals unique to their marine environment. As the sensory anatomy of cetacean glabrous skin has not been fully explored, skin biopsy samples of the flank skin of humpback whales were prepared for general histological and immunohistochemical (IHC) analyses of innervation in this study. Histology revealed an exceptionally thick epidermis interdigitated by numerous, closely spaced long, thin diameter penicillate dermal papillae (PDP). The dermis had a stratified organization including a deep neural plexus (DNP) stratum intermingled with small arteries that was the source of intermingled nerves and arterioles forming a more superficial subepidermal neural plexus (SNP) stratum. The patterns of nerves branching through the DNP and SNP that distribute extensive innervation to arteries and arterioles and to the upper dermis and PDP provide a dense innervation associated through the whole epidermis. Some NF-H+ fibers terminated at the base of the epidermis and as encapsulated endings in dermal papillae similar to Merkel innervation and encapsulated endings seen in terrestrial mammals. However, unlike in all mammalian species assessed to date, an unusual acellular gap was present between the perineural sheaths and the central core of axons in all the cutaneous nerves perhaps as mechanism to prevent high hydrostatic pressure from compressing and interfering with axonal conductance. Altogether the whale skin has an exceptionally dense low-threshold mechanosensory system innervation most likely adapted for sensing hydrodynamic stimuli, as well as nerves that can likely withstand high pressure experienced during deep dives.

Keywords

cetacean, cutaneous axons, dermis, epidermis, marine mammal, mechanosensory

Introduction

Extant cetaceans diverged from a terrestrial ancestor more than 50 million years ago (Thewissen and Williams, 2002; Uhen, 2007; Fordyce, 2018). During their evolution, cetaceans have evolved numerous adaptations to the aquatic medium, which differs from the aerial medium by an increased density, viscosity, and heat capacity, as well as rapidly changing pressure with depth. These physical properties tremendously affected the general bauplan of modern cetacean species, especially their skin, due to its direct contact with the external environment. Thus, cetaceans offer a promising system to explore specific adaptations of the skin to the aquatic environment.

Cetacean skin is generally glabrous (*i.e.*, hairless). In some species, single hairs or hairs arranged in rows or fields have been documented on the head or adjacent to the blowhole in fetuses, neonates and/or adults (Japha, 1907, 1912; Andrews, 1914, 1916; Nakai and Shida, 1948; Slijper, 1962; Ling, 1977; Mercado III, 2014; Drake et al., 2015; Reichmuth et al., this issue; Murphy et al., this issue). Researchers have speculated that the glabrous skin, which seems to be smooth in odontocetes (Wainwright et al., 2019; Bryden and Harrison, 1986; Shoemaker and Rigway, 1991), helps cetaceans optimize locomotion (Fish and Hui, 1991; Fish et al., 2008). Consequently, the rapid sloughing of the skin (Palmer and Weddell, 1964; Hicks et al., 1985) is likely an adaptation that prevents the attachment of organisms (*i.e.,* bio-fouling) and thus maintains the skin's low drag characteristics during locomotion (Fish and Hui, 1991). Other studies physiological studies in *Tursiops truncates* have measured tactile sensitivity (Strahan et al., 2019) epidermal growth rate (Hicks et al., 1985) and evoked potential response (Ridgway and Carder, 1994).

Histological examinations of cetacean skin report additional differences from terrestrial mammalian skin that can also be considered adaptations to the aquatic medium: sebaceous as well as sweat glands, unnecessary underwater, are missing (Giacometi, 1967; Greenwood et al., 1974; Sokolov, 1982; Berta et al., 2015), and cells within the cetacean epidermis contain large quantities of intracellular fat droplets, which may relate to cellular metabolism or waterproofing of the skin (Harrison and Thurley, 1972; Spearman, 1972; Knospe, 1989; Pfeiffer and Jones, 1993; Garten and Fish, 2020). Moreover, the cetacean epidermis comprises only three of the five layers commonly found in the epidermis of other mammals (Sokolov, 1955; Sokolov, 1960;

Grills et al., 1984; Morales-Guerrero et al., 2017; Garten and Fish, 2020): (1) an outermost water-resistant layer, the stratum corneum, which is not fully cornified (*i.e.*, parakeratotic), and which displays a gradual transition from live to dead cells; (2) the stratum spinosum, which contains keratinocytes with highly folded cell borders connected through desmosomes; and (3) the single-cell layer basement membrane, the stratum basale, which is connected to thick collagen bundles in the subjacent dermis. The stratum lucidum and granulosum, which typically lie between the stratum corneum and the stratum spinosum, are lacking in the cetacean epidermis.

The epidermis is an effective protective barrier from the external environment and is extremely thick in most cetaceans. In mysticetes, depending on species and body region, the epidermis can be up to 50 times thicker than in terrestrial mammals (Japha, 1905; Sokolov, 1982; Haldiman et al., 1985; Morales-Guerrero et al., 2017). Long epidermal rete ridges interdigitate with pencillate dermal papillae that can extend superficially more than half the thickness of the epidermis (Japha, 1905; Sokolov, 1960; Clarke, 1978; Sokolov, 1982; Grills et al., 1984; Haldiman et al., 1985; Knospe, 1989; Morales-Guerrero et al., 2017). This extensive interdigitation may provide mechanical stabilization to maintain skin integrity under high shear forces experienced during swimming (Knospe, 1989; Garten and Fish, 2020) and may aid cell proliferation to enable rapid regeneration of the skin surface (Grills et al., 1984; Jones and Pfeiffer, 1994).

The papillary dermis, which lies proximal to the epidermis and is reported to be thin or nearly absent in *Balaenopteridae* (Sokolov, 1960; Sokolov, 1982), contains a network of collagen and elastin fibers, often forming large bundles (Palmer and Weddell, 1964); the elastin network is described as more well-developed throughout the dermis and subcutaneous tissue in mysticetes relative to odontocetes (Sokolov, 1960; Sokolov, 1982). Together with the incomplete cornification, this network likely increases the flexibility of cetacean skin (Grills et al., 1984); but because the whale skin has air-filled spaces that may compress at depth , the skin may be deformed, and cellular locations altered which may be transduced by the somatosensory nerves. The extension and arrangement of arterioles and venules in the superficial dermis and dermal papillae has been hypothesized to mediate thermoregulation in odontocete skin (Scholander and Schevill, 1955; Palmer and Weddell, 1964). A thermoregulatory function has also been attributed to the extension of fat cells to the superficial dermis (Sokolov, 1960; Sokolov, 1982; Grills et al.,

1984), and to the extraordinarily thick cetacean hypodermis (Iverson and Koopman, 2018).

Besides the functions just mentioned, the cetacean skin most likely allows the perception of external stimuli such as nociceptive, thermo-, chemo- and mechano-sensory stimuli. Indeed, cetacean skin has been reported to be highly sensitive to tactile stimuli (Kolchin and Bel'kovich, 1973; Ridgway and Carder, 1990). In all other mammalian species, high skin sensitivity is mediated by a rich variety of innervation, including free and encapsulated nerve endings. Innervation density, as well as the morphology and density of specialized nerve endings, varies depending on body region (Palmer and Weddell, 1964; Harrison and Thurley, 1972; Yablokov et al., 1974; Bryden and Molyneux, 1986; Reeb et al., 2007; Mercado III, 2014; Berta et al., 2015; Gerussi et al., 2021; Hüttner et al., this issue). While a number of researchers have already described the innervation of the head and its sensory components in cetaceans, the innervation of the skin of the body has received less attention (Giacometi, 1967; Haldiman et al., 1985; Reeb et al., 2007; De Vreese et al., 2014). This lower level of interest is surprising as the body skin is the largest sensory organ of cetaceans. However, current hypotheses on skin function are derived from relatively broad descriptions of skin innervation and are still largely speculative. Since behavioral tests of putative functions are impractical, particularly in the large mysticetes, more detailed and refined analyses of cetacean body skin innervation and skin architecture are needed.

The interpretation of in-depth descriptions of innervation in cetacean skin can be facilitated by a direct comparison with skin innervation of terrestrial mammals, which has already been thoroughly described and successfully linked to function for some species (Rice and Albrecht, 2008b). In terrestrial mammals, dermal innervation of the body is constituted by primary sensory neurons, whose cell bodies reside in the dorsal root ganglia. These neurons are pseudo-unipolar, with an axon extending distally to peripheral targets and another axon that extends centrally to synapse on second-order neurons in the spinal cord dorsal horn gray matter. Sensory axons contain neurofilaments of which different varieties tend to be characteristic of different physiological functions. The 180-220 kDa heavy chain NF (NF-H) is typically characteristic of large-caliber, myelinated, rapidly-conducting sensory axons that are physiologically categorized as Aβ-fibers. They are low-threshold mechanoreceptors (LTMRs) with morphologically distinctive endings that are activated by different types of stimuli, including innocuous mechanical contact with the skin surface or hair follicles (Abraira and Ginty, 2013). Thinner caliber, slower conduction axons tend to have medium-chain weight NF

(NF-M), are lightly myelinated, and categorized as Aδ-fibers, while the thinnest light chain weight NF (NF-L), are unmyelinated C-fibers that terminate as morphologically nondistinct free nerve endings. The latter fibers transduce temperature and nociceptive damaging stimuli but may also respond as low-threshold mechanoreceptors (Hallin et al., 1991; Viana et al., 2002; Lewin and Moushourab, 2004; Butler and Hodos, 2005; Lumpkin and Bautista, 2005; Abraira and Ginty, 2013; Rutlin et al., 2014).

In this study, skin samples were collected from the flanks of humpback whales *(Megaptera novaengliae)*. Previous investigations of the skin of humpback whales reported some aspects on the general skin architecture with specific reference to tubercles and hairs, epidermal lipids as well as melanin (Japha, 1907, 1912; Yablokov and Klevezal, 1969; Pfeiffer and Jones, 1993; Morales-Guerrero et al., 2017). Increasing our knowledge of skin anatomy and innervation of the skin of this mysticete might be particularly informative for considering cetacean skin sensation. Given that this species is cosmopolitan, engages in diverse foraging strategies, seeks prey throughout the water column, migrates long distances, and exhibits complex social and vocal communications, the skin experiences a multitude of external conditions and may perceive a broad range of external stimuli. The current study was designed to develop a method to improve biopsy protocols for collecting marine mammal skin that preserve tissue integrity and to visualize sensory components of the glabrous skin of the humpback whale. Biopsy samples were processed for histology and immunolabeling with antibodies that indicate peripheral axons, LTMRs, glia (Schwann cells), and mechanically-gated ion channels in terrestrial mammal skin, thereby allowing descriptions of similarities and differences between terrestrial and aquatic mammal skin and inferences from skin innervation to function.

Material and methods

Subjects, permits, and tissue sampling and preparation

To visualize sensory anatomy in cetacean skin, skin samples were collected from the flanks of adult humpback whales (*Megaptera novaeangliae*; Fig. 1A) at necropsy or by biopsy under permits issued by the U.S. National Marine Fisheries Service (NMFS; Tab. 1). Skin samples were transferred under NMFS letters of authorization to S.A.E. for storage and processing at Boston University Medical Center.

Histology using Masson's trichrome stain

A sample of skin, excised at necropsy along the longitudinal axis of a stranded humpback whale (NMFS permit 10641, Tab. 1), was fixed in 10% formalin for 48 hours, dehydrated, paraffin-embedded, sectioned on a rotary microtome at 7 μm, and mounted on a gelatin-coated slide to air-dry at room temperature (RT) for 3 days. Sections from every whale in this study were then rehydrated in graded aqueous solutions prior to processing in Masson's trichrome stain (Foot, 1933), dehydrated through graded alcohols, cleared in xylene, and coverslipped with Permount (Fisher Scientific, Waltham, MA).

Tissue collection and preparation

Samples acquired for immunolabeling were biopsied from free-swimming animals following best practice methods (Clapham and Mattila, 1993; Wenzel et al., 2010; Noren and Mocklin, 2012). A specialized stainless steel biopsy dart tip was affixed to a bolt fitted with a 2.5 cm stop to ensure recoil and prevent deeper penetration. Bolts were launched from a Barnett Recruit Recurve crossbow. Dart tips were sterilized after each use and stored in 70% ethanol. Retrieved skin plugs were cylinders that measured 7 mm in diameter and about 3 cm in length (Fig. 1B). Biopsies were collected into 4% paraformaldehyde or Zamboni's fixative and stored for 48 h at 4°C, before being transferred into fresh fixative solution for an additional 48 h. Samples were then cryoprotected in successive incubations of 0.1 M phosphate buffer (PBS; pH = 7.4) and 2% dimethyl sulfoxide (DMSO), first with 10% glycerol for 48 h, and then with 20% glycerol for 48 h or until equilibrated at 4°C (Rosene et al., 1986). Plugs were flash frozen in isopentane at -75°C and stored at -80°C until cut on a sliding microtome into sections perpendicular or parallel to the skin's surface at 50 μm, 100 μm, and 200 μm. Sections were collected in PBS with 15% glycerol as cryoprotectant, equilibrated overnight at 4°C and stored at -80°C. Immediately prior to use, sections were thawed at RT and rinsed three times for 5 min in 0.05 M Tris-buffered saline (TBS) to wash off cryoprotectant. Once all plugs from flank skin of each whale were cut, multiple skin sections from all cases were processed and serial sections were used to follow axons through the depth of tissue.

Clearing lipid and melanin

A pre-treatment lipid and melanin removal protocol was performed on 100 μm and 200 μm free-floating sections. The method was modified from Mangus et al. (Mangus et al., 2016). In addition to rendering the whale's epidermal cells transparent, the technique also removed sufficient lipids to improve binding of primary antibodies, and reduced background staining in light microscopy and autofluorescence in fluorescent microscopy. The procedure was performed on a rocker at RT as follows: 15 s in reverse osmotic water (RO), 0.25% potassium permanganate in RO 30 min for 100 μm sections and 40 min for 200 μm sections, 3 s dip in RO, 2% oxalic acid dissolved in RO until epidermal cells were uniformly stained (~10 min for 100 μm sections and ~14 min for 200 μm sections), washed three times 15 min in TBS, then stored 2 days at 4°C in TBS.

Immunohistochemistry

Immunohistochemistry (IHC) was performed on free-floating 50 μm untreated and 100 μm pre-treated sections. To quench endogenous peroxidase, sections were incubated 1 hour in TBS containing 3% hydrogen peroxide (H_2O_2), and washed three times 5 min in TBS. Sections were incubated for 1 hour in a blocking solution of 10% Normal Goat Serum (NGS) and 0.4% Triton-X in TBS. Primary antibodies (specifications and concentrations described below) were mixed into a TBS solution containing 2% NGS and 0.2% Triton-X. Sections were incubated for 48 hours at 4°C with gentle agitation in the primary antibody solution, then washed three times for 5 min each in TBS with 2% NGS and 0.2% Triton-X, followed by a 2 hour incubation with secondary antibody (goat anti-rabbit or goat anti-mouse, 1:600; Vector, Burlingame, CA) in TBS containing 2% NGS and 0.2% Triton-X, washed three times for 5 min each in TBS, incubated 1 hour in an avidin biotinylated horseradish peroxidase complex (ABC Kit, Vector, Burlingame, CA), then washed three times for 5 min each in TBS. Sections selected for chromogenic development in DAB (Sigma, St. Louis, MO) were incubated in 0.55 mm DAB dissolved in TBS with 0.02% H_2O_2. Sections selected for chromogenic development with Vector-VIP (magenta) were incubated in purchased kit solutions, as described in manufacturer's directions (Vector, Burlingame, CA). Sections selected for chromogenic development with nickel-DAB were washed three times for 5 min each in 0.1 M sodium acetate, then developed in 0.05% nickel (II) sulfate and 0.55 mm DAB dissolved in TBS with 0.02% H_2O_2. Development time in the

chromogenic solution was quenched in TBS when the batch's negative control section had visible background hue, then washed three times for 5 min each in TBS. A counterstain for nucleic acids was performed on a pre-treated section (see above, lipid clearing) for 10 s in 0.5% methyl green (Sigma, St. Louis, MO) dissolved in 0.1 M sodium acetate buffer, and rinsed briefly in RO. Sections were mounted onto gelatin-coated slides, air dried, dehydrated through graded alcohols, cleared in xylene, and coverslipped with Permount (Thermo Fisher Scientific, Waltham, MA).

Fluorescent IHC and double labeling

Double fluorescent IHC was performed on 200 μm sections pre-treated to remove lipids and melanin. Free-floating tissues were preincubated 1 hour in a blocking solution of 10% NGS and 0.4% Triton-X in TBS. Sections were then incubated 48 hours at 4°C, with gentle agitation, in a solution containing primary antibodies to NF-H, and if double-labeled, S-100 (specifications and concentrations described below) in a TBS solution containing 2% NGS and 0.2% Triton-X, then washed three times for 5 min each in TBS with 2% NGS and 0.2% Triton-X. Tissues were incubated 2 hours in secondary antibodies conjugated to goat-anti-rabbit Alexafluor 488 1:1000 (catalog No. A-11034, Thermo Fisher Scientific, Waltham, MA), and if double-labeled, goat-anti-mouse IgG2a Alexafluor 633 1:1000 (catalog No. A-21136, Thermo Fisher Scientific, Waltham, MA), in TBS containing 2% NGS and 0.2% Triton-X, then washed three times for 5 min each in TBS. Sections were mounted onto gelatin-coated slides, and coverslipped with anti-fade fluorescent mounting media (PVA-DABCO, Sigma-Aldrich, St. Louis, MO).

Primary antibodies were selected based on their ability to mark known innervation in terrestrial mammalian skin. Titration trials were run to optimize antibody concentrations for visualization of targeted structures with chromogenic and fluorescent reporters (Hoffmann et al., 2008). Specific antibodies and optimized concentrations were:

1. Anti-PGP9.5 (anti-protein gene product 9.5, rabbit polyclonal, 1:1000, catalog No. PA1-46343; Thermo Fisher Scientific, Waltham, MA). The antigen is a synthetic peptide corresponding to human PGP protein purified from pathogen-free human brain consisting of residues A(176) S S E D T L L K D A A K V C R(191). Anti-PGP9.5 has been found to be a universal neuronal marker of peripheral innervation in other species, including rats (Fundin et al., 1997; Rice et al., 1997), raccoons (Rice and Rasmusson, 2000), monkeys (Pare et al., 2002),

naked mole-rats (Park et al., 2003), humans (Albrecht et al., 2006), Florida manatees (Sarko et al., 2007) and cetaceans (Gerussi et al., 2021).

2. Anti-NF-H (anti-neurofilament 200-kDa subunit, rabbit polyclonal, chromogenic IHC 1:5000 or fluorescent IHC 1:400, catalog No. PA1-10016, Thermo Fisher Scientific, Waltham, MA). The antigen was purified from neurofilament polypeptide in bovine spinal cord. The antibody labels heavy chain neurofilament, primarily the hyperphosphorylated form, with a molecular weight of 200 kDa (manufacturer's technical information). Immunolabeling for this protein has been localized to myelinated fibers, including Aβ and Aδ fibers in a variety of species, including rats (Fundin et al., 1997; Rice et al., 1997), raccoons (Rice and Rasmusson, 2000), monkeys (Pare et al., 2002), naked mole-rats (Park et al., 2003), humans (Albrecht et al., 2006), and Florida manatees (Sarko et al., 2007). Specificity of NF-H labeling was provided in these species using pre-adsorption controls and the demonstration that labeling was limited to myelinated innervation. Staining in *M. novaeangliae* skin produced axonal immunoreactivity similar to descriptions of sensory fibers in the previous studies of species listed above.

3. Anti-S100 (mouse monoclonal IgG2a antibody, chromogenic IHC 1:2000 or fluorescent IHC 1:200, catalog No. MA1-26621, Thermo Fisher Scientific, Waltham, MA). The antigen was purified from bovine brain S-100 protein. This protein has been localized to glial and ependymal cells in the brain, and Schwann cells of the peripheral nervous system (manufacturer's technical information). Immunolabeling for S100 protein has been localized to cutaneous Schwann cells and glia of other species including rats (Fundin et al., 1997; Rice et al., 1997), monkeys (Pare et al., 2002), humans (Haro et al., 1991; Reinisch and Tschachler, 2012), and Florida manatees (Sarko et al., 2007). Controls in the rat and monkey studies demonstrated that the specificity of S100 labeling was limited to glia. Staining in *M. novaeangliae* skin showed immunoreactivity identical to descriptions of Schwann cells and glia in the previous studies of species listed above.

4. Anti-ASIC2 (anti-acid sensing ion channel 2, also known as BNaC and ACCN, rabbit polyclonal, 1:500, catalog No. OSR00098W, Thermo Fisher Scientific, Waltham, MA). The antigen is a synthetic peptide from the c-terminal region of human ASIC2 neuronal structures that generate a biphasic current with a fast inactivating and a slow sustained phase. The antigen is localized at the plasma membrane of neurons, in the soma, and punctated in neuritic processes (manufacturer's technical information). The protein is associated with low-threshold

mechanoreception (Price et al., 2000; Garcia-Anoveros et al., 2001; Myers and Peltier, 2013; Cabo et al., 2015). Immunolabeling for ASIC2 has been demonstrated in the skin of monkeys (Cabo et al., 2012) and humans (Cabo et al., 2015). Staining in *M. novaeangliae* skin included structures described above, as well as diffuse, punctate and fine-fiber staining associated with fascicles.

To minimize assay variability, serial section studies were batch processed. Each IHC experiment included negative control sections processed without primary antibody, and positive control sections consisting of extraneous skin or brain tissue acquired from Rhesus macaques in previous studies (Mortazavi et al., 2016). For multi-labeling experiments, control trials were also conducted to verify there was no cross-reactivity between primary antibodies and unintended secondary targets.

Imaging acquisition, post-processing, and tracings

Sections processed with Masson's trichrome and chromogenic IHC were imaged on an E600 Nikon microscope equipped with Turboscan Montaging system (Objective Imaging, UK) using 20X and 40X objectives and Nikon's NIS Elements Advanced Research software v. 4.51, captured on a QImaging digital camera (Surrey, BC, Canada), post-processed in Adobe Photoshop (v. CS6, San Jose, CA) and adjusted so white balance was similar for each section.

Sections labelled by immunofluorescent IHC, were imaged on a Leica SPE laser scanning confocal microscope (Buffalo Grove, IL). AlexaFluor-488 emission was detected using laser excitation at 488-nm, and Alexafluor-633 emission detected with a 638-nm laser. Optical z-stack sections were collected as .LIF files using a 20x objective lens at a resolution of 1024 x 1024 pixels. The number of z-slices was determined by the system's automated optimization setting. The z-stacked .LIF files were imported into FIJI software (Schindelin et al., 2012). Individual channels were merged using the z-projection function to flatten optical z-stacks. Flattened images were adjusted with FIJI so contrast and intensity were similar for each antibody. Flattened z-stacked images for each channel (antibodies for NF-H+ and S-100+ immunoreactivity) were aligned and combined to show structures in a 600 μm tissue block. Composite images were merged to show co-labeled NF-H+ and S-100+ proteins. As a common reference, a single section of S100-stained epidermal cells (an epidermal peg) was sited in each figure. Individual axons were tracked through optical sections, and to trace axons through the

tissue block. Images collected from serial sections of IHC PGP9.5 staining, were imported into Photoshop (v. CS6, San Jose, CA). At the level of the basal epidermal depth (BED), fiber bundles were tracked and traced in red, and the basal end of epidermal pegs in black.

Results

Skin cells, tissues and vasculature

Biopsy and necropsy skin samples were collected from the flank region of *M. novaeangliae* as shown in Figure 1A. An example of a removed biopsy plug (Fig. 1B) illustrates the delineation of the cellular melanated epidermis from the underlying loose connective tissue of the dermis. At the superficial border of the hypodermis is a plexus of arteries, veins and innervation, the deep neurovascular plexus (DNP) (Fig.2C). The DNP is located with the reticular dermis, the deepest dermal strata. It has fewer and smaller adipocytes than the hypodermis, and more collagen and fibroblasts. In this study, a neurovascular plexus was discovered superficial to the reticular dermis, in the deep region of the overlying papillary dermis, and named the papillary neurovascular plexus (PNP). Its vasculature contains arterioles and venules. Between the reticular dermis and basal epidermis is the papillary dermis, rich in collagen and fibroblasts, with small and sparse adipocytes (Fig 2.).

At the junction of the papillary dermis and basal epidermis is the most distal plexus, the subepidermal neurovascular plexus (SNP), with thin-walled arterioles and venules. Projections of dermis invaginate into the epidermis, forming the cetacean's distinct, pencillate dermal papillae. Dimensions and proportions of the papillae and epidermis vary by body region and species, although the taxon's epidermis is thicker than in other mammals (>25 mm in bowhead whales, *Balaena mysticetus*; Haldiman et al., 1985). In the humpback whale skin, pencillate dermal papillae were densely packed and very long extending almost through the full thickness of the epidermis as had been observed previously (>13mm in bowhead whales; Haldiman et al., 1985). Capillaries of the papillae originate in the SNP, to oxygenate the epidermis, and mediate thermoregulation.

The deepest epidermal layer is the single cell layer of heterogeneous cells, the stratum basale. These cells are separated by intercellular gaps, but linked together by a basement membrane tethered to thick bundles of compact collagen in the underlying dermis. Superficial to

the stratum basale is the cetacean's major epidermal strata, the stratum spinosum. Lipokeratinocytes are the resident cells of the cetacean's stratum spinosum. These cells have high lipid content and deeply folded borders connected by desmosomes that restrict seawater infiltration making the outer epidermis a tough water-resistant barrier (Scholander and Schevill, 1955; Sokolov, 1955; Haldiman et al., 1985; Knospe, 1989; Reeb et al., 2007) (Fig. 2).

Specific cells, tissues and structures of *M. novaeangliae* skin were visualized with Masson's Trichrome stain (Fig. 2A, 2B) and with immunohistochemistry using the antibody to PGP9.5, a pan-axonal marker (Fig. 2C). As shown in Figure 2A, the epidermis is about 10 mm thick with three epidermal strata: corneum, spinosum, and basale. Superficially, dense sheets of cornified cells form the distal stratum corneum (Fig. 2A). Melanokeratinocytes, the major epidermal cells, comprise the stratum spinosum. The well-organized compact layer of stratum basale cells borders the dermis. Collagen fibrils anchor the superficial dermis to the stratum basale (Fig. 2B). Strata lucidum and granulosum are not present in *M. novaeangliae* skin. Pencillate dermal papillae ascend from the dermis into the epidermis where they interdigitate with epidermal pegs. Measurements of *M. novaeangliae* skin show that the dermal papillae are 7 mm in length and 80-120 μm in diameter (Fig. 2A).

Dermal-epidermal junction (DEJ)

The dermal-epidermal junction (DEJ) is the boundary plane at the base of the epidermal pegs, tangential to the skin's surface (Fig. 2A, B). The shape of some epidermal pegs is affected by the presence of adjacent vasculature. Contiguous with the dermis of the papillae, the papillary dermis continues for ~800 μm deep to the DEJ and is inclusive of the superficial network of neurovascular bundles that form the SNP. Deep to the SNP is the reticular dermis. This layer exhibits fewer collagen fibers and an increase in adipocyte size and density and ranges from ~0.8 - 2.3 mm deep to the DEJ. At the deep junction with the hypodermis, it meets another network of neurovascular bundles, the DNP. This plexus is characterized by neurovascular bundles with larger vessels. These vessels course superficially to the hypodermis. The well-vascularized SNP and DNP supply branches of arterioles and venules to the DEJ and capillaries that extend apically through the length of the dermal papillae.

Deep neural plexus and reticular dermis

The DNP is filled by thick-walled arteries (Fig. 3A, B) as well as accompanying veins. In Figure 3A, the pan-axonal marker PGP9.5 reveals a thick network of PGP9.5+ axons surrounding an artery. This network is 25 μm thick and includes NF-H+ Aβ-fibers (Fig. 3G) that are mechanosensory. Large fascicles branch into smaller fascicles, dividing the nerve fiber bundle into daughter bundles with fewer nerve fibers (Fig. 3A). Perineurial cells stained by PGP9.5 form the perineurium (Fig. 3C-E) and reveal an apparent unfilled space between the axon bundle and perineurium (Fig. 3C–3E). Staining with the antibody to NF-H confirms these axons are sensory fibers. As expected, NF-H did not mark the perineurium, although background tissue was faintly stained and delineated the fascicle space (Fig. 3F).

Multi-labeling immunofluorescence was used to co-localize—low-threshold mechanoreceptor (LTMR) Aβ-fibers, identified by NF-H, together with Schwann cells and neuropil marked by α-S100. Optical Z-stack sections collected on a confocal microscope show axons, forming a network of linear NF-H+ fibers (Fig. 3G) surrounding a large vascular space. This is contrasted with the diffuse staining patterns of S-100+ Schwann cells (Fig. 3H). The fluorescent markers confirm these are sensory nerve fibers (marked by NF-H) associated with Schwann cells and their processes (marked by S-100; Fig. 3I).

Subepidermal neural plexus and papillary dermis

The SNP is ~600-800 μm beneath the DEJ (Fig 2A, 2C). A dense sensory nerve fiber network, ~20 μm thick, surrounds arteries in the plexus (Fig. 4). Cross-sectional cuts show nerve fiber bundles contacting the arterial vasculature (Fig. 4A-4C). Nerve fiber bundles departing the neurovascular network may split into smaller bundles (Fig. 4B). Conversely, multiple fascicles extending away from an arterial wall also join larger fascicles (Fig 4C). Fascicles also intersected, with nerve fibers branching off the bundle (Fig. 3D).

As in the DNP, fascicles of the SNP have an apparently empty space (Fig. 4D-4F). Nerve fiber bundles tend to cluster in a small area within the fascicle, adjacent to the perineurial wall. However, individual nerve fibers also occur in close association with the perineurial wall, separated from the bundled nerve fibers (Fig. 4E). Fine neurofilaments embedded in the perineurium connect with the nerve fiber bundle associated with the opposing perineurial wall (Fig. 4F).

Fibers at the dermal-epidermal junction

At the DEJ, NF-H+ nerve fiber bundles approach, branch, and interact with the epidermis in diverse patterns. Figure 5A shows NF-H+ in the SNP branching into a dermal papilla. Fascicles and axons also directly contact the basal end of epidermal pegs (Fig. 5B). The section in Figure 5C was cleared of melanin to label S100+ glia, including Schwann cells and their processes, and also perineurial cells. The intrafascicle space between the fibers and perineurium also shows diffuse S-100+ reactivity. The nickel-DAB stain reveals multiple fibers contact a single point on the basal end of a peg (Fig. 5D). Fiber bundles are also observed traveling from the base of one epidermal peg to the next (Fig. 5E).

Figure 6 is the result of a multi-labeling experiment showing flattened z-stack images, acquired from three 200 μm serial sections. Flattened images were aligned and merged to show the morphology of axon bundles in a 600 μm block of skin. This optical reconstruction reveals a complex, previously undescribed axon morphology at the DEJ. A bundle of seven NF-H+ fibers forms two adjacent nerve loops at the basal end of an epidermal peg, diverging into dermal papillae on opposing sides of the peg (Fig. 6A-6D). Co-localization with S100+ confirms the presence of Schwann cells surrounding the mechanosensory fibers (Fig. 6E, 6F). One nerve loop is round and the other flattened into a long triangular shape against the epidermis (Fig. 6G).

Fiber tracings through the aligned optical sections reveal that the orientation of the fibers is the same in both loops. Action potential propagation would likely travel from terminals in the epidermis down the axon toward the CNS as suggested by the arrows in Figure 6H. Axon diameters of these Aβ-axons have a broad range in diameter, 0.6 – 2.3 μm, consistent with a collection of fibers with different mechanosensory properties (Fig. 6I).

Serial section tracing of multiple fibers contacting the DEJ (Fig. 7) illustrate multiple patterns of fiber associations with the epidermal pegs and dermal papillae. Overall, ten different patterns are observed (Fig. 7). These patterns include fibers contacting the basal end of epidermal pegs, bundles branching in the papillary dermis, fibers contacting multiple epidermal pegs, and fiber bridges traversing across the dermal papillae between the epidermal walls (Fig. 7A-J).

Axon morphology in the dermal papillae

The complex fiber trajectories within the dermal papillae explained in the previous paragraph afford potential sensory fiber contacts with the epidermal sidewalls (Fig. 8A). What

appears to be a novel end bulb contact with an epidermal wall is shown in Figure 8B. While most sensory fibers travel longitudinally in the center of the dermal papillae (Fig 8B), some traversed between opposing sidewalls (Fig. 8C). Cross-sections of dermal papillae in melanin-cleared skin show LTMR as NF-H+ Aβ-fibers (Fig. 8D) and S100+ Schwann cells surrounding the nerve fibers with immune-response cells in the stratum basale (Fig. 8E). Other diverse fiber forms included splaying, tortuous tangled loops and simple loops along the epidermal wall (Fig. 8F-8H). Proceeding distally, the perineurial wall of fascicles thinned. Figure 8F shows the fascicle and intrafascicle space, faintly contrasted against the connective tissue. Tortuous axon formations were apparent in the center of the papillae (Fig. 8G). Simple loops were only observed in contact with the epidermis (Fig. 8G). Fiber bundles were seen targeting a single cell of the stratum basale, then proceeding apically (Fig. 8I). Staining with nickel-DAB showed LTMR Aβ-fibers embedded in the stratum basale (Fig. 8J). In a melanin-cleared section, α-S100 immunoreactivity revealed a rare Meissner's-like morphology in the apex of a dermal papilla, along with Schwann cells supporting the axons and stacked lamellar cells (Fig. 8K).

Figure 9A shows NF-H+ fibers forming a bridge-like crossing between the epidermal walls as they ascend in the core of a short papilla. An adjoining epidermal peg is contacted at the base by another fascicle with the Aβ-fibers forming a bulb (Fig. 9B) while the superficial end of the dermal papillae contains a single Aβ fiber in contact with the cells of the stratum basale.

LTMR ion channels and fibers

Immunoreactivity to α-ASIC2 identified LTMR ion channels as well as many fine-caliber fibers in fascicles subjacent to the basal tip of epidermal pegs (Fig. 10A).

Discussion

Neural structures labeled by antibodies to terrestrial mammalian innervations demonstrate a robust system of afferent fibers. These molecular homologues, with known sensory function in well-studied land mammals, are presumed to perform similar roles in whales.

In this study, the cutaneous innervation was described for the flank skin of *M. novaeangliae*. Our findings demonstrate that humpback whales skin contains a high density of cutaneous innervation as revealed by α-PGP immunolabeling, which is the most comprehensive

of all known labels for all types of peripheral innervation. This included the full range of sensory fiber types from the relatively slowest conducting, thinnest unmyelinated C fibers to the fastest conducting, largest caliber myelinated Aβ fibers. Positive α-HNF+, α-S100, and α-ASIC2 immunolabeling as biomarkers indicate the presence of the LTMR contingent, which would be of particular relevance to detecting hydrostatic pressure and different types of hydrostatic wave transduction in the marine environment. Other functional types of innervation labeled by α-PGP, but lacking positive immunolabelling with additional biomarkers, presumably are involved in different types of nociceptive, thermal, and chemical transduction, which could be of future interest and assessed by using other functionally related biomarkers.

Unlike glabrous terrestrial skin (Rice and Albrecht, 2008b), end organs that transduce high-resolution stimuli were nearly absent from *M. novaeangliae* skin, and individual fibers did not branch. Instead, fibers traveled from the dermis in bundles that make contact with the epidermis at the base or along the walls of the dermal papillae. In the study species, the discrete endings that transduce somatic stimuli in land mammals have been replaced with a novel system of branching fascicles that likely subserve diverse functions including a means for detecting complex stimuli, such as flow velocities, pressure differentials, and/or tissue compressions that may be related to swim speeds and dive depth. Future work should focus on somato-sensory responses in other cetaceans in order to assess whether the findings obtained in *M. novaeangliae* are also evident in other mysticetes and perhaps common to cetaceans in general.

Neurovascular organization of humpback whale skin

Dermal strata are delineated by the neurovascular plexuses that separate the hypodermis, reticular dermis, and papillary dermis (Fig. 2). The skin of *M. novaeangliae* is richly innervated with mechanosensory Aβ-fibers traveling in dense networks around arteries in the DNP (Fig. 3A, 3B, 3G-I) and SNP (Fig. 4A). Some NF-H+ fiber bundles and fascicles immediately diverge into multiple directions (Fig. 4B) while others assemble into larger fascicles (Fig. 4C). Capillary networks extend all the way into the dermal papillae providing thermoregulation and nutrients for the thick epidermis (Fig. 8B, 8D, 8E).

Intrafascicle space: functional considerations

In the peripheral nervous systems of terrestrial mammals (Rice and Albrecht, 2008b),

nerve fascicles are densely packed with axons, Schwann cells, myelin and the collagenous fibers of the endoneurium (CN). Fascicles can be observed in all derma strata in the flank skin of the whale, however, there is an area that seems to be devoid of nerve fibers and glial, at least as detected by the IHC in this study. Both α-PGP and α-S-100 antibodies mark glia (perineurial cells) that form the perineurium. Staining with α-PGP shows that within the perineurium there is an apparently empty space, lacking PGP+ axons, in the reticular dermis (Fig. 3C-E), papillary dermis (Fig. 4D-F, 5B), and dermal papillae (Fig. 8F). Even S-100+ Schwann cells surrounding fibers in the superficial dermal papillae do not fill the intra-perineurium void (Fig. 5C). The fascicle space was also visible with NF-H+ labeled LTMR fibers (Fig. 3F). Assuming this unstained area is indeed unoccupied, it appears that about 56-64% of the cross sectional area is not filled. To our knowledge, this intrafascicle space has not been described in the skin of other species or in other neural systems.

In cross-sectional views, PGP+ fiber bundles showed a tendency to cluster near the perineurium (Fig. 4D - 4F). Opposing sides of the fascicle had small PGP+ axons attached to perineurium, that connected with the fiber bundle (Fig. 4E, 4F). Additionally, we observed LTMR ASIC2+ ion channels on axons that embedded in the perineurium. (Fig. 10; Cabo et al., 2013). The presence of fibers located near the walls of these fascicles that are positive for mechanically gated channels raises the possibility that these mechanically gated channels are linked to components of the extracellular matrix, and may be highly tuned to movement of the fascicle relative to the extracellular matrix (Cabo et al., 2012; Cabo et al., 2015; Poole et al., 2015). Here, we propose that the fascicle with its perineurium may be an anchoring substrate for sensory nerves and might even constitute a specialized end organ unique to the whale.

A particularly unique feature of the nerves in the humpback was a non-cellular gap between the perineurial sheath and the core bundle of axons which has not been observed in other species previous. We do not know the non-cellular physical property of this gap but it may be some sort of displaceable component, perhaps even a gas, that may protect the axons from being compressed and blocking their conductance under extreme hydrostatic pressure.

Adaptations and roles of fiber bundles

Parallel bundles of tightly aligned axons were persistent throughout the dermis while single axons were seen only occasionally in dermal papillae. Overall, axonal bundles exhibited

diverse patterns. Extending fiber bundles often divided, and occasionally merged, throughout the dermis (Fig. 4B-D, 6, 7, 9A). Traveling bundles contacted the basal end of multiple epidermal pegs tangential to the skin's surface (Fig. 5E, 7C), and frequently made contact with the epidermal wall at multiple depths (Fig. 8A). Entire bundles were also seen targeting a single cell on the basal end of an epidermal peg (Fig. 5D) and in a sidewall projection of a dermal papilla (Fig. 8I).

Fiber bundles also formed complex structures. Mechanosensory Aβ-fibers, identified with NF-H along with Schwann cells identified by PGP, appeared to travel between neighboring dermal papillae, forming adjoining loops at the basal end of their shared epidermal peg. In tracing these fibers through the z-dimension, it was noted that these fibers had the same directionality into and out of the loop. As shown in Figure 6, fibers of two loops merged and ascended as a seven-fiber bundle. This organization might allow for integration across multiple dermal papillae.

Unlike the thin stratified skin of land mammals that has individual branching axons and a few discreet end organs, the whale's axons travel in tight, parallel multi-afferent bundles, enclosed within a fascicle and ensheathing perineurium. From the deep to distal dermis, axons persist within bundles. Immunolabeling revealed a variety of novel and complex three-dimensional structures, bifurcations, and contact patterns with the dermal-epidermal junction. While we did not observe any axons branching, specializations in the papillae included bridges, tangled and simple loops, and rarely, end-bulbs or a Meissner's-like corpuscle. The deep region of each dermal stratum has a neurovascular plexus, transporting dense matrices of low-threshold mechanosensory fibers.

This cetacean system of fascicles may be an adaptation that supports conduction velocity by maintaining axons without nodes and thinning branches. The parallel fibers may also serve to amplify signaling, compare signal intensity, or time of arrival. Specialized nerve endings in encapsulated organs may subserve fine-scale discriminative tactile resolution in terrestrial mammals may be unnecessary on the flank of a large aquatic mammal. While in terrestrial mammals, dermal axons are sinuous and winding in glabrous skin, and straight and taught in hairy skin, in whale skin, the fascicular organization appears to be intermediate to terrestrial glabrous and hairy skin (Fig. 5B-5D, 8A, 8B) (Provitera et al., 2007).

Dermal papillae as specialized endings

Encapsulated sensory end organs that subserve fine-scale sensation have fibrous capsules that surround nerve termini and support cells, provide increased sensory ending that facilitate signal transduction by afferent axons (Cauna, 1956a, 1956b; Cauna and Ross, 1960; Saxod, 1996; Vega et al., 1996; Bensmaia, 2002; Fleming and Luo, 2013). In humpback whale skin, tubular dermal papillae may be an alternative specialization that also facilitates transduction of stimuli unique to the cetacean aquatic environment. Loose connective tissue of the papillae is surrounded by collagenous fibers embedded in the basement membrane of the stratum basale wall (Fig. 2B). External vibrations and physical forces are transmitted through the dense epidermis to axons on the interior wall of the papillae and within the collagen fiber matrix.

While the pattern of neural structures within papillae varies, results from this study show the matrix of innervated papillae is a relevant property of cetacean skin. Corpuscular end organs of vertebrate skin are rare in the flank skin of humpback whales but not absent. A string of fibers with bulbous endings terminated within a papillae core and apical stratum basale (Fig. 8B). Similar bulbous endings were found within Meissner's corpuscles of human digits (Nolano et al., 2003). A Meissner's-like ending was also seen in the apex of a papilla. Anti-S100 marked the glia and stacked lamellar cells consistent in the prototypical shape and location of the Meissner's corpuscle (Del Valle et al., 1993; Rice and Albrecht, 2008a; Garcia-Suarez et al., 2009). Ending types that were morphologically similar to those in terrestrial mammals consisted of regularly occurring likely Merkel endings that terminate among the basal layer of the epidermis, and small encapsulated endings and likely Meissner corpuscles that were present in, but rarely observed among the PDP. In terrestrial mammals, Merkel nerve endings serve as mechanoreceptors, providing information on mechanical pressure, position, and deep static touch features, such as shapes and edges (Lumpkin and Bautista, 2005; Rice and Albrecht, 2008b; Abraira and Ginty, 2013) and a similar function is likely in whales. Otherwise, most of the large proportion of LTMR endings, aside from those detected on arteries and arterioles, were concentrated in dermal papillae as morphological tangles and/or fibers that were in close contact with the epidermis over most of the length of the PDP. These were also present but not as prevalent as in larger terrestrial species such as raccoons, pigs, monkeys and humans (Rice and Rasmusson, 2000; Pare et al., 2002; Albrecht et al., 2006; Rice and Albrecht, 2008b).

Humpback whale skin as an underwater tactile sensory system

The immunohistochemical methods in this study describe cetacean skin innervation from the flank region (Fig. 1A), which opens new approaches to understanding the skin structure and function in large aquatic mammals that occupy diverse habitat types. These aquatic mammals are also exposed to environmental stress from pollution and climate change. Skin is the ever present prime point of contact and barrier to the waters that form the essential environment of these animals. In this paper, we explored the morphology of the largest sensory element of one species of baleen whales; i.e., skin, in great detail. We also offered hypotheses for the functionality and significance for the unique features found in this morphometric study of humpback whale skin. The findings are consistent with a well-integrated and sensitive tactile sensory system that may efficiently monitor hydrodynamic parameters such as ambient pressure, water flow, and temperature changes (Pawlowicz, 2013). These potential functions remain to be exactingly explored and tested across multiple species of cetaceans to understand how skin sensations may integrate or inform other sensory systems in whales. Equally important, these findings need to be compared with similar studies for other species of marine mammals such as sireneans (manatees, dugongs) and pinnipeds (seals and sea lions) that are sensitive to hydrodynamic perception and face a similar physical environment to determine whether there are parallel or divergent adaptations across taxa (Hanke et al., 2013; Gaspard et al., 2013).

Acknowledgments

Regrettably, the senior author, Sherri Eldridge, died before this manuscript could be submitted and published. Her co-authors on this paper have therefore worked to assure Eldridge's research was documented and published on her behalf posthumously. The following acknowledgements are those which Dr. Eldridge wrote in appreciation for the efforts of many individuals to achieve this complex and extensive project.

We would like to acknowledge the technical assistance of the laboratory members at Boston University School of Medicine (BUSM), Department of Anatomy and Neurobiology: Eli Shobin, Tara L. Moore, Bethany Bowley, Penny Schultz, Karen L. Slater, Rebecca Smith, Joe Herbert, Samantha M. Calderazzo, Katelyn Trecartin and Ajay Uprety. For assistance with tissue collection and permits, we thank the National Marine Fisheries Service (NMFS), Hawaiian Islands Humpback Whale National Marine Sanctuary, Stellwagen Bank National Marine Sanctuary, Pacific Islands Fisheries Science Center (NMFS permit #15240), Marine Mammal

Stranding Network, Doug Nowacek (Duke University, NMFS permit # 14809), Rachel Finn, Ka'au Abraham, Michael Thompson, Tammy Silva, Laura Howes, and Mason Weinrich. We also thank Michael Moore and Woods Hole Oceanographic Institution for paraffin embedded skin samples (NMFS #10641). Special thanks for financial and research support by NOAA's Dr. Nancy Foster Scholarship Program, National Marine Sanctuaries, Kate Thompson, Mitchell Tart, Seaberry Nachbar, and Steve Gittings. We also thank Thermo Fisher Scientific for antibodies.

Funding

Grant sponsor: National Ocean Service, Grant number NA10SEC4810008 (to S.A.E); Grant sponsor: NIH, Grant numbers R01-AG043640, R01-AG042512 (to D.L.R.); Grant sponsor: American Association of University Women; Grant: American Dissertation Fellowship (to S.A.E).

Conflict of interest

The authors declare that there are no conflict of interests, singly nor collectively.

Permits

S.A.E. holds letters of authorization from the U.S. National Marine Fisheries Service (NMFS) to receive and study whale tissues collected by, or under the supervision of, NMFS take permit holders. Research was conducted at Boston University Medical Center.

Literature cited

Abraira VE, Ginty DD. 2013. The sensory neurons of touch. Neuron 79:618-639.

Albrecht PJ, Hines S, EIsenberg R, Pud D, FInlay DR, Connolly MK, Pare M, Davar G, Rice FL. 2006. Pathologic alterations of cutaneous innervation and vasculature in affected limbs from patients with complex regional pain syndrome. Pain 120:244-266.

Andrews RC. 1914. Monographs of the Pacific cetacea I. The California gray whale *(Rhanchianectes glaucus* Cope*)*. Memoirs of the American Museum of Natural History 1:227-287.

Andrews RC. 1916. Monographs of the Pacific cetacea. II. The sei whale *(Balaenoptera borealis* Lesson*)* 1. History, habits, external anatomy, osteology, and relationship. Memoirs of the American Museum of Natural History 1:289-388.

Bensmaia S. 2002. A transduction model of the Meissner corpuscle. Math Biosci 176:203-217.

Berta A, Ekdale EG, Zellmer NT, Demere TA, Kienle SS, Smallcomb M. 2015. Eye, nose, hair, and throat: external anatomy of the head of a neonate gray whale (Cetacea, Mysticeti, Eschrichtiidae). Anatomical record 298:648-659.

Bryden and Harrison. Research on Dolphins. Oxford, UK: Oxford University Press, 1986.

Bryden MM, Molyneux GS. 1986. Ultrastructure of encapsulated mechanoreceptor organs in the region of the nares. In: Bryden MM, Harrison RJ, editors. Research on dolphins. Oxford: Clarendon Press. p 99-107.

Butler AB, Hodos W. 2005. Comparative vertebrae neuroanatomy: evolution and adaptation. Hoboken, New Jersey: John Wiley & Sons, Inc.

Cabo R, ALonso P, Vina E, Vazquez G, Gago A, Feito J, Perez-Molto FJ, FGarcia-Suarez O, Vega JA. 2015. ASIC2 is present in human mechanosensory neurons of the dorsal root ganglia and in mechanoreceptors of the glabrous skin. Histochemistry and Cell Biology 143:267-276.

Cabo R, Galvez A, Laura R, San Jose I, Pastor JF, Lopez-Muniz A, Garcia-Suarez O, Vega JA. 2013. Immunohistochemical detection of the putative mechanoproteins ASIC2 and TRPV4 in avian herbst sensory corpuscles. Anat Rec (Hoboken) 296:117-122.

Cabo R, Galvez MA, San Jose I, Laura R, Lopez-Muniz A, Garcia-Suarez O, Cobo T, Inausti R, Vega JA. 2012. Immunohistochemical localization of acid-sensing ion channel 2 (ASIC2) in cutaneous Meissner and Pacinian corpuscles of *Macaca fascicularis*. Neuroscience Letters 516:197-201.

Cauna N. 1956a. Nerve supply and nerve endings in Meissner's corpuscles. Am J Anat 99:315-350.

Cauna N. 1956b. Structure and origin of the capsule of Meissner's corpuscle. Anat Rec 124:77-93.

Cauna N, Ross LL. 1960. The fine structure of Meissner's touch corpuscles of human fingers. J Biophys Biochem Cytol 8:467-482.

Clapham PJ, Mattila DK. 1993. Reactions of humpback whales to skin biopsy sampling on a West Indies breeding ground. Mar Mamm Sci 94:382-391.

Clarke MR. 1978. Structure and proportions of the spermaceti organ in the sperm whale. Journal of the Marine Biological Association of the United Kingdom 58:1-17.

De Vreese D, Doom M, Haalters J, Cronilie P. 2014. Heeft de uitwendige gehoorgang van walvisachtigen nog enige functie? Vlaams Diergeneeskundig Tijdschrift 83:284-292.

Del Valle ME, Cabal A, Alvarez-Mendez JC, Calzada B, Haro JJ, Collier W, Vega JA. 1993. Effect of denervation on lamellar cells of Meissner-like sensory corpuscles of the rat. An immunohistochemical study. Cell Mol Biol (Noisy-Le-Grand) 39:801-807.

Drake SE, Crish SD, George JC, Stimmelmayr R, Thewissen JGM. 2015. Sensory hairs in the bowhead whale, *Balaena mysticetus* (Cetacea, Mammalia). Anatomical record 298:1327-1335.

Fish FE, Howle LE, Murray MM. 2008. Hydrodynamic flow control in marine mammals. In: Annual meeting of the Society for Integrative and Comparative Biology. San Antonio, Texas. p 788-800.

Fish FE, Hui CA. 1991. Dolphin swimming - a review. Mammal Review 21:181-195.

Fleming MS, Luo W. 2013. The anatomy, function, and development of mammalian Abeta low-threshold mechanoreceptors. Frontiers in biology 8.

Foot NC. 1933. The Masson trichrome staining methods in routine laboratory use. Biotechnic and Histochemistry 8:101-110.

Fordyce E. 2018. Cetacean evolution. In: Würsig B, Thewissen JGM, Kovacs KM, editors. Encyclopedia of marine mammals, 3 ed. London San Diego Cambridge Oxford: Academic press. p 180-185.

Fundin BT, Pfaller K, Rice FL. 1997. Different distributions of the sensory and autonomic innervation among the microvasculature of the rat mystacial pad. Journal of Comparative Neurology 389:545-568.

Garcia-Anoveros J, Samad TA, Zuvela-Jelaska L, Woolf CJ, Corey DP. 2001. Transport and localization of the DEG/ENaC ion channel BNaC1alpha to peripheral mechanosensory terminals of dorsal root ganglia neurons. Journal of Neuroscience 21:2678-2686.

Garcia-Suarez O, Montano JA, Esteban I, Gonzalez-Martinez T, Alvarez-Abad C, Lopez-Arranz E, Cobo J, Vega JA. 2009. Myelin basic protein-positive nerve fibres in human Meissner corpuscles. J Anat 214:888-893.

Garten JL, Fish FE. 2020. Comparative histological examination of the integument of odontocetes flukes. Aquatic Mammals 46:367-381.

Gaspard JC 3rd, Bauer GB, Reep RL, Dziuk K, Read L, Mann DA. 2013. Detection of hydrodynamic stimuli by the Florida manatee (Trichechus manatus latirostris). J Comp Physiol A Neuroethol Sens Neural Behav Physiol. 199(6):441-50. doi: 10.1007/s00359-013-0822-x. Epub 2013 May 10. PMID: 23660811.

Gerussi T, Graic J-M, De Vreese S, Grandis A, Tagliavia C, De Silva M, Huggenberger S, Cozzi B. 2021. The follicle-sinus complex of the bottlenose dolphin *(Tursiops truncatus).* Functional anatomy and possible evolutional significance of its somato-sensory innervation. Journal of Anatomy 238:942-955.

Giacometi L. 1967. The skin of the whale *(Balaenoptera physalus)*. Anatomical Record 159:69-76.

Greenwood AG, Harrison RJ, Whitting HW. 1974. Functional and pathological aspects of the skin of marine mammals. In: Harrison RJ, editor. Functional anatomy of marine mammals, Volume 2. New York: Academic Press. p 73-110.

Grills JJ, Skoch EJ, Hoste R. 1984. Comparative histological investigations of the epidermis of five species of cetaceans. IAAAM. https://www.vin.com/apputil/content/defaultadv1.aspx?pId=11100&id=3981624

Haldiman JT, Henk WG, Henry RW, Albert TF, Abdelbaki YZ, Duffield DW. 1985. Epidermal and papillary dermal characteristics of the bowhead whale *(Balaena mysticetus)*. Anatomical Record 211:391-402.

Hallin RG, Ekedahl R, Frank O. 1991. Segregation by modality of myelinated andunmyelinated fibers in human sensory nerve fascicles. Muscle Nerve 14:157-165.

Hanke, W., Wieskotten, S., Marshall, C. *et al.* (2013). Hydrodynamic perception in true seals (Phocidae) and eared seals (Otariidae). *J Comp Physiol A* **199,** 421–440. doi.org/10.1007/s00359-012-0778-2

Haro JJ, Vega JA, del Valle ME, Calzada B, Zaccheo D, Malinovsky L. 1991. Immunohistochemical study of sensory nerve formations in human glabrous skin. European Journal of Morphology 29:271-284.

Harrison RJ, Thurley KW. 1972. Structure of the epidermis in *Tursiops*, *Delphinus*, *Orcinus* and *Phococena*. Journal of Anatomy 111:498-500.

Hicks BD, St Aubin DJ, Geraci JR, Brown WR. (1985). Epidermal growth in the bottlenose dolphin, Tursiops truncatus. J Invest Dermatol. 85(1):60-3. doi: 10.1111/1523-1747.ep12275348.

Hoffmann GE, Le WW, Sita LV. 2008. The importanve of titrating antibodies for immunocytochemical methods. Current Protocols in Neuroscience doi: 10.1002/0471142301.ns0212s45.

Iverson S, Koopman HN. 2018. Blubber. In: Würsig B, Thewissen JGM, Kovacs KM, editors. Encyclopedia of marine mammals, 3 ed. London San Diego Cambridge Oxford: Academic press. p 107-110.

Japha A. 1905. Über den Bau der Haut des Seihwales *Balaenoptera borealis* (Lesson). Zoologischer Anzeiger 29:442-445.

Japha A. 1907. Über die Haut nord-atlantischer Furchenwale. Zoologische Jahrbücher Abteilung für Anatomie und Ontogenie der Tiere 24:1-40.

Japha A. 1912. Die Haare der Waltiere. Zoologische Jahrbücher Abteilung für Anatomie und Ontogenie der Tiere 32:1-42.

Jones FM, Pfeiffer CJ. 1994. Morphometric comparison of the epidermis in several cetacean species. Aquatic Mammals 20:29-34.

Knospe C. 1989. Zur Wasseranpassung der Walhaut - Histologische und histochemische Untersuchung bei Delphin, *Delphinus delphis*, und Schweinswal, *Phocaena phocaena*. Anatomia Histologia Embryologia 18:193-198.

Kolchin S, Bel'kovich V. 1973. Tactile sensitivity in *Delphinus delphis*. Zoologicheskiv Zhurnal 52:620-622.

Lewin GR, Moushourab R. 2004. Mechanosensation and pain. Journal of Neurobiology 61:30-44.

Ling JK. 1977. Vibrissae of marine mammals. In: Harrison RJ, editor. Functional anatomy of marine mammals. London: Academic Press. p 387-415.

Lumpkin EA, Bautista DM. 2005. Feeling the pressure in mammalian somatosensation. Current Opinion in Neurobiology 15:382-388.

Mangus LM, Dorsey JL, Weinberg RL, Ebenezer GJ, Hauer P, Laast VA, Mankowski L. 2016. Tracking epidermal nerve fiber changes in Asian macaques: tools and techniques for quantitative assessment. Toxicologic Pathology 44:904-912.

Mercado III E. 2014. Tubercles: what sense is there? Aquatic Mammals 40:95-103.

Morales-Guerrero B, Barragán-Vargas C, Silva-Rosales GR, Ortega-Ortiz CD, Marinez-Levasseur LM, Acevedo-Whitehouse K. 2017. Melanin granules melanophages and a fully-melanized epidermis are common traits of odontocete and mysticete cetaceans. Veterinary Dermatology 28:213-e250.

Mortazavi F, Wang X, Rosene DL, Rockland KS. 2016. White matter neurons in young adult and aged Rhesus monkey. Frontiers in Neuroanatomy 10:15.

Myers MI, Peltier AC. 2013. Uses of skin biopsy for sensory and autonomic nerve assessment. Current Neurology and Neuroscience Reports 13:323.

Nakai J, Shida T. 1948. Sinus hairs of the sei-whale *(Balaenoptera borealis)*. Scientific Reports of the Whale Research Institute 1:41-47.

Nolano M, Provitera V, Crisci C, Stancanelli A, Wendelschafer-Crabb G, Kennedy WR, Santoro L. 2003. Quantification of myelinated endings and mechanoreceptors in human digital skin. Ann Neurol 54:197-205.

Noren DP, Mocklin JA. 2012. Review of cetacean biopsy techniques: Factors contributing to successful sample collection and physiological and behavioral impacts. Mar Mamm Sci 28:154-199.

Palmer E, Weddell G. 1964. The relationship between structure, innervation and function of the skin of the bottlenose dolphin *(Tursiops truncatus)*. Proceedings of the Zoological Society of London 143:553-567.

Pare M, Smith AM, Rice FL. 2002. Distribution and terminal arborizations of cutaneous mechanoreceptors in the glabrous finger pads of the monkey. Journal of Comparative Neurology 445:347-359.

Park TJ, Comer C, Carol A, Lu Y, Hong HS, Rice FL. 2003. Somatosensory organization and behavior in naked mole-rats: II. Peripheral structures, innervation, and selective lack of neuropeptides associated with thermoregulation and pain. Journal of Comparative Neurology 465:104-120.

Pawlowicz R. 2013. Key physical variables in the ocean: temperature, salinity, and density. Nature Education Knowledge 4:13.

Pfeiffer CJ, Jones FM. 1993. Epidermal lipid in several cetacean species: ultrastructural observations. Anatomy and Embryology 188:209-218.

Poole K, Moroni M, Lewin GR. 2015. Sensory mechanotransduction at membrane-matrix interfaces. Pflugers Arch 467:121-132.

Price MP, Lewin GR, McIlwrath SL, Cheng C, Xie J, Heppenstall PA, L. SC, G. MA, Brennan TJ, Drummond HA, Qiao J, Benson CJ, Tarr DE, Hrstka RF, Yang B, Williamson RA, Welsh MJ. 2000. The mammalian sodium channel BNC1 is required for normal touch sensation. Nature 407:1007-1011.

Provitera V, Nolano M, Pagano A, Caporaso G, Stancanelli A, Santoro L. 2007. Myelinated nerve endings in human skin. Muscle Nerve 35:767-775.

Reeb D, Best PB, Kidson SH. 2007. Structure of the integument of Southern right whales, *Eubalaena australis*. Anatomical Record 290:596-613.

Reinisch CM, Tschachler E. 2012. The dimensions and characteristics of the subepidermal nerve plexus in human skin--terminal Schwann cells constitute a substantial cell population within the superficial dermis. Journal of Dermatological Science 65:162-169.

Rice FI, Fundin BT, Arvidsson J, Aldskogius H, Johansson O. 1997. Comprehensive immunofluorescence and lectin binding analysis of vibrissal follicle simus complex innervation in the mystacial pad of the rat. Journal of Comparative Neurology 385:149-184.

Rice FL, Albrecht PJ. 2008a. Cutaneous mechanisms of tactile perception: Morphological and chemical organization of the innervation to the skin. In: Basbaum AI, Kaneko A, Shepherd GM, Westheimer G, editors. The Senses, A Comprehensive Reference. San Diego, CA: Academic Press. p 1-32.

Rice FL, Albrecht PJ, editors. 2008b. Cutaneous mechanisms of tactile preception: morphological and chemical organization of the innervation to the skin. San Diego: Academic Press.

Rice FL, Rasmusson DD. 2000. Innervation of the digit on the forepaw of the raccoon. Journal of Comparative Neurology 417:467-490.

Ridgway SH, Carder DA. 1990. Tactile sensitivity, somatosensory responses, skin vibrations, and the skin surface ridges of the bottlenose dolphin, *Tursiops truncatus*. In: Thomas J, Kastelein R, editors. Sensory abilities of cetaceans. New York: Plenum Press. p 163-179.

Ridgway, S.H., & Carder, D.A. (1994). Auditory-evoked potentials for assessment of hearing in marine animals. *Journal of the Acoustical Society of America, 96*, 3269-3269.

Rosene DL, Roy NJ, Davis BJ. 1986. A cryoprotection method that facilitates cutting frozen sections of whole monkey brains for histological and histochemical processing without freezing artifact. J Histochem Cytochem 34:1301-1315.

Rutlin M, Ho CY, Abraira VE, Cassidy C, Woodbury CJ, Ginty DD. 2014. The cellular and molecular basis of direction selectivity of Adelta-LTMRs. Cell 159:1640-1651.

Sarko DK, Reep RL, Mazurkiewicz JE, Rice FL. 2007. Adaptations in the structure and innervation of follicle-sinus complexes to an aquatic environment as seen in the Florida manatee *(Trichechus manatus latirostris)*. The Journal of Comparative Neurology 504:217-237.

Saxod R. 1996. Ontogeny of the cutaneous sensory organs. Microsc Res Tech 34:313-333.

Schindelin J, Arganda-Carreras I, Frise E, Kaynig V, Longair M, Pietzsch T, Preibisch S, Rueden C, Saalfeld S, Schmid B, Tinevez JY, White DJ, Hartenstein V, Eliceiri K, Tomancak P, Cardona A. 2012. Fiji: an open-source platform for biological-image analysis. Nature Methods 9:676-682.

Scholander PF, Schevill WE. 1955. Counter-current vascular heat exchange in the fins of whales. Journal of Applied Physiology 8:279-282.

Shoemaker, P.A., & Ridgway, S.H. (1991). CUTANEOUS RIDGES IN ODONTOCETES. *Marine Mammal Science, 7*, 66-74.

Slijper EJ. 1962. Whales. New York: Basic Books.

Sokolov V. 1960. Some similarities and dissimilarities in the structure of the skin among members of the suborder *Odontoceti* and *Msytacoceti* (*Cetacea*). Nature 185:745-747.

Sokolov VE. 1955. Structure of the integument of some cetaceans. Byulleten' Moskovskogo Obshestva Ispitatelej Prirodi Otdel Biologii 60:45-60.

Sokolov VE. 1982. Mammal skin. Berkeley, Los Angeles, London: University of California Press.

Spearman RIC. 1972. The epidermal stratum corneum of the whale. Journal of Anatomy 113:373-381.

Strahan, M.G., Houser, D.S., Finneran, J.J., Mulsow, J., & Crocker, D.E. (2020). Behaviorally measured tactile sensitivity in the common bottlenose dolphin, Tursiops truncatus. *Marine Mammal Science, 36*, 802-812.

Thewissen JGM, Williams EM. 2002. The early evolution of Cetacea (whales, dolphins, and porpoises). Annual Review of Ecology and Systematics 33:73-90.

Uhen MD. 2007. Evolution of marine mammals: back to the sea after 300 Million years. Anatomical Record 290:514-522.

Vega JA, Haro JJ, Del Valle ME. 1996. Immunohistochemistry of human cutaneous Meissner and pacinian corpuscles. Microsc Res Tech 34:351-361.

Viana F, de la Pena E, Belmonte C. 2002. Specificity of cold thermotransduction determined by differential ionic channel expression. Nature Neuroscience 5:254-260.

Wainwright DK, Fish FE, Ingersoll S, Williams TM, St Leger J, Smits AJ, Lauder GV. 2019. How smooth is a dolphin? The ridged skin of odontocetes. Biology letters 15:10190103.

Wenzel F, Nicolas J, Larsen F, Pace RM, III. 2010. Northeast Fisheries Science Center Cetacean Biopsy Training Manual. In: U.S. Department of Commerce N, National Marine Fisheries Service, editor. Woods Hole, MA: Northeast Fisheries Science Center

Yablokov AV, Klevezal GA. 1969. Whiskers of whales and seals and their distribution structure, and significance. In: Kleinenberg SE, editor. Morphological characteristics of aquatic mammals. Moscow: Isdatel'stvo "Nauka".

Yablokov AV, M. BV, Borisov VI. 1974. Whales and dolphins, Part II. Joint Publication Research Service 62150-1:286.

FIGURE LEGEND

Fig. 1. Sample location of flank skin in M. novaeangliae. (A) Lateral trunk (mid-dorsal body wall) area sampled for tissue biopsy and necropsy. (B) Biopsy plug (7 mm diameter x 25 mm). Coloration differentiates dark epidermal strata corneum and spinosum and stratum basale from the white papillary dermis and hypodermis. Locations of stratum corneum and stratum basale are marked with dashed lines. Scale bar A = 1 m; B =7mm. Whale art by Fiona Reid

Fig. 2. Histology of M. novaeangliae skin. (A) Vertical section of plug stained with Masson's trichrome. The epidermis is interdigitated with 5-7 mm long pencillate dermal papillae (DP), ~100 μm in diameter. The dermal-epidermal junction (DEJ) is seen in the horizontal plane at the basal tip of the epidermal pegs (EP). PD – papillary dermis, RD – reticular dermis, HY – hypodermis. (B) Representative enlargement at the DEJ. Melanokeratinocytes (MK) form the stratum spinosum. Dense collagen fibrils (CL, blue) are oriented parallel to the stratum basale (SB). A capillary (CA) occupies the center of a DP. A little deeper is a superficial layer of adipocytes (AD) and beneath that is the subepidermal neural plexus, characterized by the presence of both arterioles (ARt) and skeletal muscle cells (SMC, red). (C) This section was immunostained for PGP9.5+ for morphological features, and reveals nerve fibers (arrowheads), nerve fascicles (FA), arteries (AR) as well as venous spaces (VS). It also reveals the subepidermal neural plexus (SNP) at the lower boundary for the papillary dermis and a deep

neural plexus (DNP) at the boundary of the reticular dermis with the hypodermis. Scale bar A = 1 mm; B = 100 μm; C = 300 μm

Fig. 3. Deep neural plexus (DNP) and reticular dermis: arteries, fascicles and nerve fibers. M. novaeangliae skin was immunolabeled with antibodies to PGP9.5 (Schwann cells and neurites) (A-E) or NF-H (axonal marker, myelinated fibers) (F). Background staining reflects extended development time in DAB. More superficial regions are at the top of images. (A) Cross-section of a thick-walled artery (AR) in the DNP surrounded by PGP9.5+ sensory fibers (arrowheads). Fibers branching (asterisk) from a fascicle as it travels vertically. (B) Bend in an artery shows two cross-sections of the smooth muscle cell layer and nerve fibers (arrowheads) surrounding the periphery. Collagen fibrils (CL) give structural support to neurovascular bundles within the reticular matrix of adipocytes (AD). (C-E) Perineurium (PN) forming wall around the fascicle containing an intrafascicle "space" (FA) containing nerve fiber bundles (arrowheads) as seen in longitudinal (C), cross-section (D) and oblique (E) views. The FA "space" is likely filled with an insulating layer of fat (perhaps myelin) possibly from neural support cells (neuropil). (F) Immunoreactivity to NF-H is expressed by axons, but not the perineurium. (G-I) Reconstructed z-stacks from 100 □m section, visualized with fluorescent reporters. (G) Vascular space (VS) is a artery, and surrounded by NF-H+ fibers in a > 40 μm thick network. A nerve fiber bundle (upper right) branches to or from the periphery. (H) Shows diffuse network of S-100+ support cells surrounding the vessel. (I) Merged image show co-localization (white) of nerves and Schwann cells. Scale bar: A = 100 μm; B, G-I = 50; C-D = 25 μm; E-F = 10 μm

Fig. 4. Subepidermal neural plexus (SNP) arteries, fascicles and fibers. (A) Flattened z-stack images of NF-H+ axons. (A) Cross-sectional (right - AR) and oblique (left - AR) cuts through arteries and surrounding axons. Fiber bundles project into the dermal matrix (arrowheads). (B) Fibers coalesce as they diverge to contact or enter an arterial wall (ARW). (C-F) PGP9.5+ sensory fibers (arrowheads) and perineurium (PN). (C) Chromogenic IHC reaction with nickel-DAB shows fascicles contacting an artery after leaving (asterisks) a single thick fascicle (FA). (D) Intersecting fascicles share a fiber. (E) Cross-section of a fascicle shows clustering of fibers near the perineurial wall (right arrowhead), individual axons embedded in the opposite wall (left arrowheads), and intrafascicle space (FA). (F) Thin fibers and tissue sheaths (arrowheads)

connect the interior wall of the perineurium with fascicle fibers. Scale bar: A, C = 100 μm; D = 50 μm; E = 25 μm; B, F = 10 μm

Fig. 5. Fibers and fascicles approach epidermal pegs and dermal papillae at the dermal-epidermal junction (DEJ). Axons (arrowheads), epidermal peg (EP), dermal papilla (DP), and fascicles (FA). (A) NF-H+ axons form a fiber network as they travel between the subepidermal neural plexus (SNP) and a dermal papilla. (B) PGP9.5+ fibers within a fascicle (FA) bounded by the perineurium (PN, dashed line) at the basal end of an epidermal peg. (C) Melanin-cleared section shows S100+ Schwann cell myelination of fibers within a fascicle (perineurium - dashed line). Intrafascicle material is lightly stained. (D) Four PGP9.5+ fibers contact a single point at the basal end of an EP. (E) PGP9.5+ fibers appear in close apposition with the basal end of neighboring epidermal pegs (arrowheads). Scale bar: A = 100 μm; B, E = 25 μm; C, D = 10 μm

Fig. 6. Axons contact basal epidermal pegs as well as distal targets in dermal papillae. (A-C) Flattened optical z-stacks were collected from three 200 μm serial sections of M. novaeangliae skin immunolabeled with NF-H and a fluorescent reporter. (D) Sections aligned and merged showing full organization of these fibers. (E) Aligned composite image of S-100+ component acquired and reconstructed from sections in A-C. Note the diffuse appearance of S-100 Schwann cells compared with distinct edges of NF-H+ fibers. (F) Merged image from D and E showing co-localization of NF-H+ sensory fibers and S-100+ Schwann cells. (G) Enlargement of boxed area in D distinguishes a triangular bundle loop (right) and round bundle loop (left). (H) Tracings of PGP9.5+ and NF-H+ fiber bundles in two colors. Arrows show possible directionality of action potential conductance to and from these two fascicles. Both fiber bundles could conduct action potentials from their contacts with the basal EP surface to the CNS although polarity of these fibers relative to body axes is unknown. (I) Diameter of fibers in each bundle. Scale bar: A-F = 75 μm; G-H = 25 μm

Fig. 7. Tracings show the diverse patterns of fiber association with the dermal-epidermal junction. (A-J) Structures were traced through serial sections at the DEJ. The basal end (stratum basale) of epidermal pegs (ep) were outlined in black, and PGP9.5+ fibers in red. Each red line represents 1-4 fibers. (A) Fiber bundle travels apically in the center of a dermal papilla (dp). (B)

Fiber bundle in the DP contacts stratum basale of epidermis at DP apex. (C) Fiber bundle in the dermis contacts stratum basale at the base of adjacent epidermal pegs. (D) Fiber bundle contacts the base of one epidermal peg and then enters a dermal papilla contacting the stratum basale of another epidermal peg. (E) Fiber bundle in dermal papilla splits to contact both the stratum basale of an epidermal peg and the apex of a dermal papilla. (F) Fiber bundle contacts the base of an epidermal peg and then splits to ascend in two adjacent dermal papilla. (G) Fiber bundle splits in the dermis to ascend in two adjacent dermal papilla. (H) Fiber bundle splits in dermis and contacts the base of adjacent epidermal pegs. (I) Fiber bundle splits in dermis and contacts stratum basale at multiple points on the same epidermal peg. (J) Fiber bundle in the papilla splits in the dermal papilla and contacts stratum basale of the epidermis at different locations on the dermal papilla apex. Scale bar = 500 μm

Fig. 8. Neural architecture and specializations in the dermal papillae (DP). Sensory axons marked with antibodies to PGP9.5 (A, B, F, G, I), to NF-H (C, D, H, J), and Schwann cells marked with antibodies to S-100 (E, K). Chromagen reactants: DAB (A-I), nickel-DAB (J), and Vector-VIP (K). Melanin was cleared from select sections (D-H, K). All images oriented with superficial areas at the top. (A) Lateral walls of the epidermal pegs (EP) may be smooth (right) or have pocketed evaginations (left). Fiber bundles can have multiple contacts along the lateral epidermal wall (lefthand arrowheads), or progress centrally in the dermal papilla (DP) to the apex (righthand arrowhead). Vascular space (VS), papillary dermis (PD). (B) End bulbs (EB) occur at fiber termini within a dermal papilla, and at the epidermal wall (white arrowhead). (C) Multi-fibers cross from one side to the other of this DP, contacting a 50 μm length along one wall (left), and 5 μm area of the opposing wall (right). (D) Cross-section of a DP about 4 mm superficial to the DEJ. Immunoreactivity to NF-H, expressed with an extended development time in DAB, shows a traveling fiber bundle and fiber in a side-wall evagination (arrowheads), stratum spinosum (SS), stratum basale (SB), thick and thin-walled capillaries (CA). (E) Similar view of section shows S-100+ glia and epidermal cells. The arrow heads mark S-100+ fibers (F) Bundled fibers in a fascicle have branches that my contact different structures along their course contact targets (arrowheads) along the path of the nerve fiber bundle. (G) Tortuous, tangled nerve fibers coursing vertically in the center of the dermal papilla. One fiber shows thickening at the point of extreme angulation (arrow), perhaps indicating it has twisted on itself (doubling

thickness), or it has a sensory bulb. (H) Fibers loop (arrowhead) along the DEJ (dashed line). (I) Fiber bundle runs in DP until it contacts a single S-100+ cell of an EP (arrow), and then continues distally (arrowhead). (J) Fibers traveling in DP make contact with the EP wall in multiple locations (arrowheads). (K) Schwann cells fibers (arrowhead) and lamellar cells (LC) of a rare Meissner's-like structure, found in the apex of a DP. Scale bar: A = 50 μm; B-E, K = 25 μm; F-J = 10 μm. NMFS (A-E) 15240, (F-K) 14809

Fig. 9. Sensory fiber formation at level of dermal-epidermal junction below truncated dermal papilla. NF-H+ fibers developed in a nickel-DAB reaction. (A) Epidermal peg (EP) is truncated above the dermal-epidermal junction (double-headed arrows). Large diameter fascicle (dashed outline), abutting basal ends of the EPs, contains mechanosensory fibers. Immunoreactive densities (dark staining) are present in stratum basale of basal ends of the EPs (white arrowheads). Adjoining dermal papilla (DP, to the right) is uncharacteristically short, □0.3 mm, and exhibits extensive innervation. (B) Enlargement of fascicle in A. Three braided nerve fibers loop to form a cord, 15 μm dia and 5 μm long then proceed to approach the basal end of an EP (white arrowhead). Superficial end of encircling fibers (black arrowhead) was not in this section. A separate axon proceeds on a parallel trajectory (arrows) to the adjacent EP's basal end. There is a white area at the junction of the nerve fibers and the EP's stratum basale. (C) Enlargement of DP apex in A. Paired fiber bridges link the opposing epidermal walls at the apex of the short DP. Chromagen is nickel-DAB. Scale bar: A = 100 μm; B, C = 25 μm

Fig. 10. Low-threshold mechanosensory ion channels are localized in the perineurium. In a melanin-cleared section of M. novaeangliae skin, ASIC2+ structures are visualized with Vector-VIP (magenta). (A) mechanoreceptive ion channels appear as purple dots on a diffusely stained fascicle (FA). (B) Densely marked area subjacent to epidermal peg (EP; box) is enlarged to clarify ASIC2+ ion channels (arrowheads). Scale bar: A = 50 μm; B = 10 μm. NMFS 15240

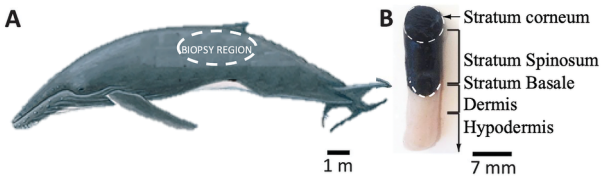

AR_24856_Figure-1.tif

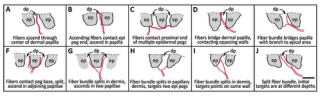

AR_24856_Figure-7.tif

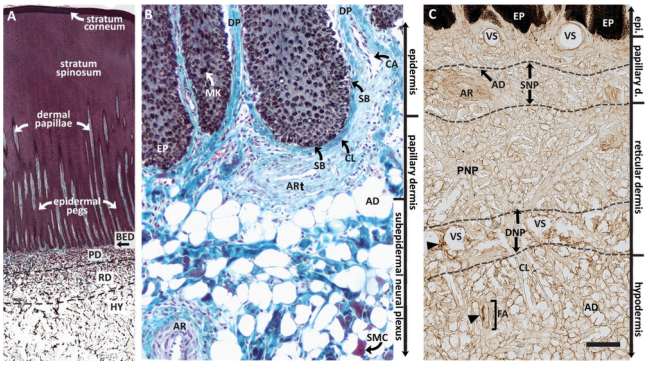

AR_24856_Figure 2.tif

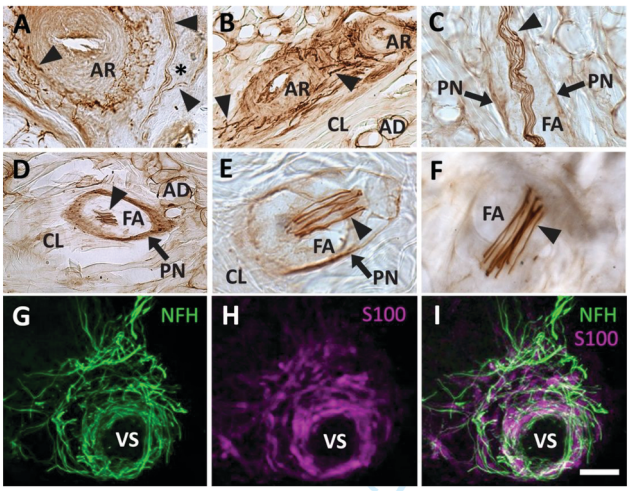

AR_24856_FIGURE 3.tif

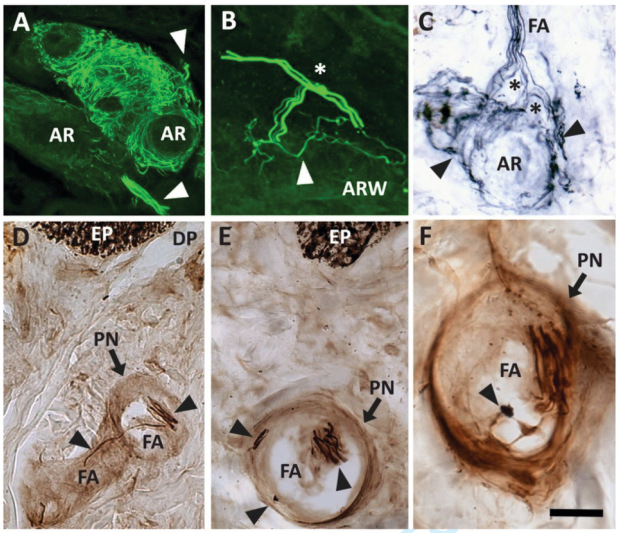

AR_24856_FIGURE 4.tif

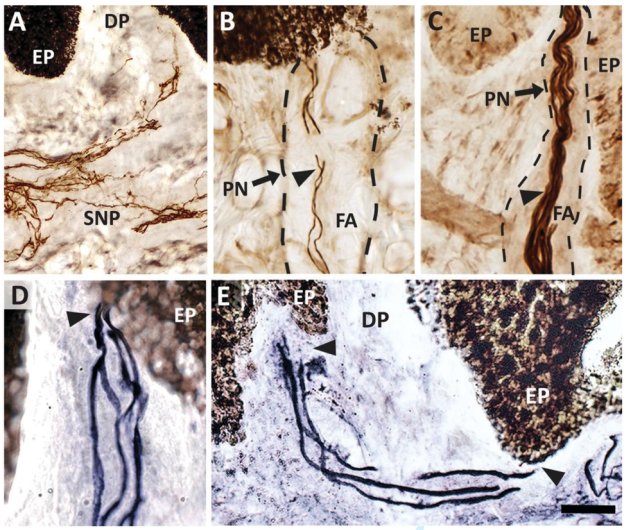

AR_24856_FIGURE 5.tif

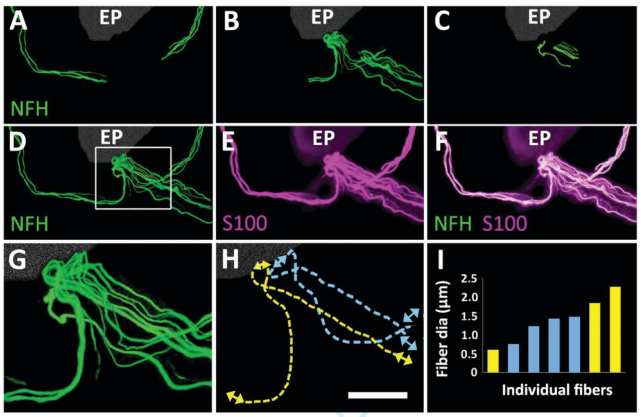

AR_24856_FIGURE 6.tif

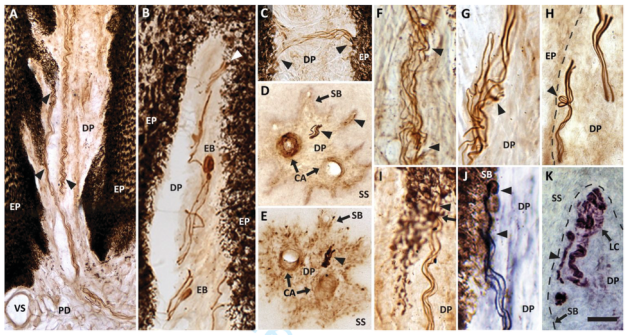

AR_24856_FIGURE 8.tif

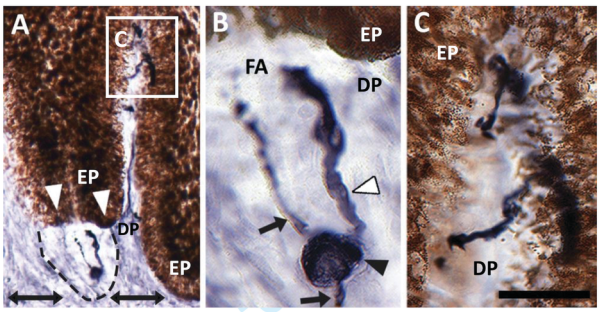

AR_24856_FIGURE 9.tif

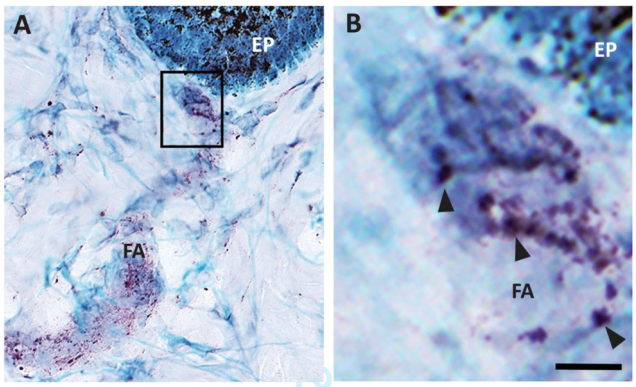

AR_24856_FIGURE_10.tif

Table 1 Overview of the subjects, humpback whales (*M. novaeangliae*), from which skin samples were taken. The table indicates the specific subject, the related National Marine Fishery Service permit number, the agency, the whale ID, the sex and maturity status as well as whether samples were collected at necropsy or by biopsy

Subject	NMFS	Agency[1]	Whale ID	Sex[2]	Maturity	Method
98-292 (1998)	10641	WHOI	98-292	F	Neonate	Necropsy
SB-13-2015	14809	SBNMS	Unknown	U	Adult	Biopsy
HI-201 (2013)	15240	HINMS	Unknown	M	Adult	Biopsy
HI-203 (2013)	15240	HINMS	Unknown	M	Adult	Biopsy
HI-303 (2013)	15240	HINMS	Unknown	M	Adult	Biopsy

[1] WHOI = Woods Hole Oceanographic Institution, Woods Hole, MA; SBNMS = Stellwagen Bank National Marine Sanctuary, Scituate, MA, Collection conducted under NMFS permit 14809, Doug Nowacek (Duke University); HINMS = Hawaiian Islands Humpback Whale National Marine Sanctuary, Maui, HI. Collection conducted under NMFS permit 15240, Pacific Islands Fisheries Science Center

[2] F = female, M = male, U = unknown

AR_24856_Table 1.tif